

Generation and propagation of underwater noise from marine propellers

Kostas Belibassakis

School of Naval Architecture & Marine Engineering,
National Technical University of Athens, Greece.

Summary

Main contributors to underwater noise generated from commercial ships are the main engines and auxiliaries (like shaft, reduction gears etc), as well as hydrodynamic interaction of hull flow in calm water and in waves, and finally, the propeller, which usually constitutes the most important source. In this work, a numerical model is developed to study non-cavitating and blade sheet cavitation noise generated from marine propellers operating in unsteady inflow conditions, at the stern of the ship. The hydrodynamic part is analyzed by a velocity-based panel method, providing the unsteady pressure on the blades and sheet cavitation data. The latter are subsequently used, in conjunction with Kirchhoff's formulation concerning radiation from moving surfaces, to predict the acoustic spectrum at several diameters distance from the propeller, representing the source of marine propeller noise. At a first level of approximation, a reduced-order model is used, exploiting information concerning the time history of blade sheet cavity and the unsteady blade forces. Results concerning cavity volume and blade thrust variations are used to calculate the monopole and dipole components of the propeller acoustic spectrum in the low and moderate frequency band. The directivity characteristics the ship propeller are calculated, and its effect on underwater noise propagation is studied comparatively to the omnidirectional source assumption.

PACS no. 43.30, 43.50

1. Introduction

Commercial ships contribute significantly to the overall background noise in the sea; see, e.g., Hildebrand (2009), McKenna et al (2012). In particular, shipping noise is considered byproduct of standard ship operations, generated from propellers, but also from main engines, machinery and flow-hull interaction, especially in waves. Noise due to machinery is more significant at low ship speeds, whereas propeller noise is dominant at high speeds, especially under cavitating conditions (AQUO 2015). On the other hand, the hydro-dynamic flow noise can be considered to be negligible far from the vessel.

The importance of shipping noise and its impact on the marine environment is demonstrated by the fact that at low frequencies below 300 Hz, ambient noise levels have been increased by 15–20dB over the last century (McKenna et al 2012), and various studies, covering the period 1950–2007, suggest that the current trends of low frequency noise increase levels in the ocean are approximately 3.3 dB per decade Frisk (2012). It is shown that the above trend is related to

commercial shipping activity and global economic growth. Furthermore, number, size and speed of ships increase continuously and lead to ever increasing noise levels. Particularly, in the frequency range from 10 to 300 Hz the natural background noise level is raised by 20 to 30dB (Wittekind et al 2009). On the side of mitigation measures, IMO has recently issued guidelines for the reduction of underwater noise from commercial shipping to address adverse impacts on marine life (IMO MEPC.1/Circ.833, 2014), including technical guidelines for the designers, shipbuilders and ship operators to minimize underwater radiated noise from ships and identifying the following key areas: propellers, hull design, onboard machinery, and operational and maintenance.

The generated noise from ship machinery and auxiliaries comes mainly from the subparts of the propulsion system. Diesel engines along with the shaft and reduction gears create a noise signature which depends on ship speed (AQUO 2015). Radiated noise related to diesel motor consists of frequencies corresponding to rotation rate and its harmonics. Auxiliary machinery noise (from compressors, generating sets, pumps, steering rear,

cooling sets, ventilation fans, air conditioning systems etc) is also an important component of radiated noise. As it can be easily understood, rotating auxiliary machinery and other equipment contribute to the overall ship acoustic signature but at lower levels than the main propulsion system (see, e.g. IMO MEPC 59/19, 2009). On the other hand, the propeller as a major source of underwater noise, as it rotates in the wake of the ship, is subjected to unsteady loads, which under specific conditions leads to cavitation; see, e.g., Kinnas et al (2003), and Seol et al (2005).

In this work, a numerical method is developed to model non-cavitating and blade sheet cavitation noise generated from marine propellers operating in unsteady inflow conditions, at the stern of the ship. The hydrodynamic part is analyzed by a velocity-based panel method, using vortex elements (Belibassis & Politis 1998), providing the unsteady pressure on the blades and sheet cavitation data. The obtained results are subsequently used, in conjunction with Kirchhoff's formulation concerning radiation emission from moving surfaces (Farassat, & Myers 1988, Farassat 2001), to predict the acoustic spectrum at several diameters distance from the propeller, representing the source of marine propeller noise.

A reduced-order model is developed, based on information concerning the time history of the blade sheet cavity shape and volume and the unsteady blade forces. More specifically, data concerning cavity volume and blade thrust variations are used to calculate the monopole and dipole components of the propeller acoustic spectrum, focusing on the low frequency band. Subsequently, the directivity characteristics of the emitted noise are examined, including the reflective effects of nearby boundaries as the ship hull, which are expected to strongly influence the underwater noise propagation in the marine environment comparatively to the omnidirectional source assumption.

2. Unsteady propeller analysis

The hydrodynamic analysis of marine propellers and the prediction of performance in inhomogeneous inflow conditions, representing the wake of the ship, is based on a velocity-based

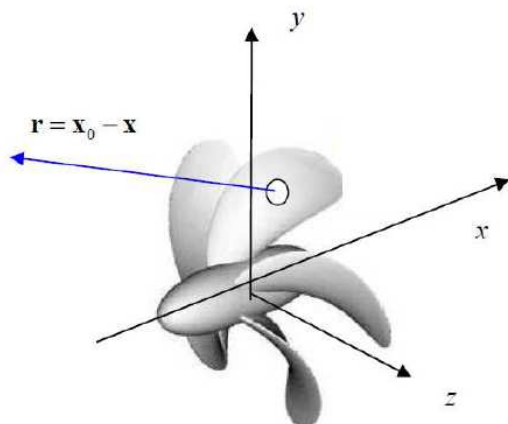


Fig.1. Propeler geometry

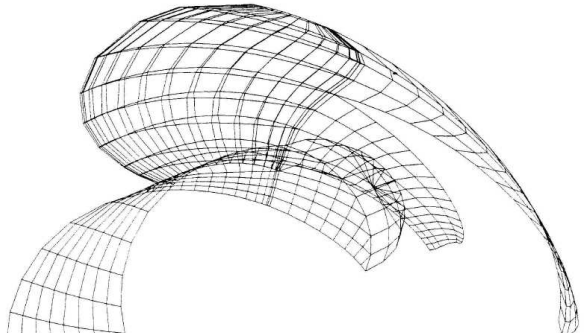


Fig. 2 Representation of propeller blade and wake by boundary elements.

boundary element method, developed by Belibassis & Politis (1998), which is extended to include propeller blade sheet cavitation effects. Each symmetrical part of the propeller consists of the blade and the hub sections; see Fig.1. Individual parameterization is introduced for the representation of each section. The complete propeller discretization is obtained by matching the grids of the particular sections. Each section of the boundary surface is subdivided into a collection of boundary, bilinear, 4-node elements, selected for the approximation of the geometry; see Fig.2. A piecewise constant scheme is utilized for the approximation of the unknown function on the boundary. To account for the effects of trailing vorticity, a free vortex sheet downstream the lifting sections of the blades has been incorporated to the model. Since the geometry of this additional boundary is unknown, it has to be determined as part of the solution. However, if the shape of the hydrodynamic trailing vortex sheets is assumed known (by means of wake model), the problem can be

approximately reduced to an integral equation over the solid surface coupled with the Kutta condition, which substantially accelerates the numerical solution. At a next level, a wake relaxation method can be applied to incorporate the nonlinear effects (see Kinnas et al 1990). According to this method some initial wake geometry is assumed for which wake grid panels are defined. For unsteady problems, the time-stepping method is applied for the solution. In this case the grid representing the free wake surface is dynamically evolving with time, as, e.g. presented by Politis (2004).

Wake models are usually constructed exploiting information from experimental observations and measurements of the relative flow quantities downstream the propeller, and by making systematical use of the non-linear numerical tools in the case under consideration. Following previous research (Kerwin & Lee 1978, Hoshino 1990), the initial part of the propeller blade vortex sheets is mathematically represented by smooth surfaces constituting the blade-wake transition region. The ultimate wake region is either a generalized helicoidal surface or it degenerates into two sets of rolled-up hub and tip vortices per blade, representing experimental observations concerning the deformation of the propeller blade vortex sheets, at increased blade loading conditions. The radial distribution of the hydrodynamic pitch angle is selected to be given by a simplified formula, (Politis & Belibasakis, 1990), in terms of the main geometrical and hydrodynamic parameters. Within the transition wake region, trailing vortex lines emanate from the trailing edge of each blade aligned to the local trailing edge angle bisector. Subsequently, moving in the downstream direction, they gradually deform to smoothly match the ultimate wake trailing vortex lines. In the case of the deformed wake model an additional contraction of the blade wake is superimposed.

2.1 Boundary Value Problem

The propeller blades are considered to be a set of symmetrically arranged thin blades, rotating with a constant angular velocity about a common axis in an unbounded, incompressible fluid. It is also assumed the blades to operate in a known incoming velocity field $\mathbf{A}(\mathbf{x})$ corresponding to the wake of the ship, at a small angle of attack, and that the spatial variation of the ship wake is

small. The blade boundary layer and shed vortex wake thickness is assumed to be thin so that the fluid rotation due to the propeller is confined in a thin layer. The presence of extraneous boundaries such as the rudder, and the ship hull, are neglected, except that the last is recognized as a body generating the non-uniform flow field.

The wake non-uniformity, due to hull boundary layer, results in the existence of spatial vorticity in propeller plane. The problem is approximately treated by separating the velocity field in two terms: the first one refers to the rotational wake whereas the second refers to perturbation velocity due to the existence of propeller, which can be considered irrotational outside the blade boundary layer. In this case the Euler equations can be numerically integrated, giving us a decoupled formulation for the propeller disturbance problem and the calculation of propeller velocity and pressure fields; see Belibasakis & Politis (1998). As it has already been mentioned, we consider a propeller operating in an unbounded, incompressible fluid, either in a non-cavitating or cavitating condition. The principle of conservation of mass is the governing equation throughout the fluid encompassing the blades, the shed wake, and the cavity. The total fluid velocity \mathbf{w} in the propeller frame of reference (see Fig.1) is given by

$$\mathbf{w} = \mathbf{U} + \mathbf{A} + \boldsymbol{\Omega} \times \mathbf{x} + \mathbf{u}, \quad \mathbf{u} = \nabla \Phi, \quad (1)$$

where \mathbf{U} and $\boldsymbol{\Omega}$ are propeller translation and rotation speed, respectively, and \mathbf{u} is the disturbance velocity field, presenting discontinuity on the trailing vortex sheets. The latter is obtained as solution of the Laplace equation for the disturbance flow potential

$$\nabla^2 \Phi = 0, \quad (2)$$

outside the propeller blades and the propeller blade wakes (trailing vortex sheets), and the cavity surface. The problem concerning the unknown disturbance potential is solved by imposing the following boundary conditions:

2.1.1 Tangency condition on the blade surface

In a blade-fixed coordinate system rotating with the propeller the impermeability condition on the wetted surface is described as:

$$\mathbf{n} \cdot \mathbf{u} = -\mathbf{n} \cdot (\mathbf{U} + \mathbf{A} + \boldsymbol{\Omega} \times \mathbf{x}), \quad (3)$$

where, \mathbf{n} is the vector normal on the blade surface.

Using the following representation for the disturbance velocity field

$$\mathbf{u}(\mathbf{x}_0) = \frac{1}{4\pi} \int_{S_B \cup S_C} \frac{\sigma \mathbf{r}}{r^3} dS(\mathbf{x}) + \frac{1}{4\pi} \int_{S_B \cup S_W} \gamma \times \frac{\mathbf{r}}{r^3} dS(\mathbf{x}), \quad (4)$$

where $\mathbf{r} = \mathbf{x}_0 - \mathbf{x}$, σ is surface source-sink distribution defined by the right-hand side of Eq.(3) on the blade and cavity surface, and γ the surface vorticity on the blade and wake surface. Using the above in the boundary condition Eq.(3), it results in the following integral equation

$$\frac{\gamma}{2} - \mathbf{n} \times \int_{S_B} \gamma \times \frac{\mathbf{r}}{4\pi r^3} dS(\mathbf{x}) = \mathbf{n} \times \int_{S_B \cup S_C} \frac{\sigma \mathbf{r}}{4\pi r^3} dS(\mathbf{x}) + \mathbf{n} \times \int_{S_W} \gamma \times \frac{\mathbf{r}}{4\pi r^3} dS(\mathbf{x}), \quad (5)$$

with respect to the surface vorticity on the propeller blades. The above representation ensures the satisfaction of condition at infinity at each time step, in the form that at large distances from the propeller, the perturbation velocity due to the presence of the propeller and cavity vanishes.

2.1.2 Kutta condition at the trailing edge

In the case of ideal flow, Kutta condition prevents the existence of infinite velocities at the trailing edge. In the present necessitating equal pressure as the trailing edge is approaches from both sides of the blade surface and provides us information concerning the vorticity field on the blade wake (last term of right-hand side of Eq.5) in terms of the solution of the integral equation in previous time steps. More specifically a relation is obtained for the spanwise vorticity shed from the trailing edge of the blade in terms of the temporal variation of the circulation around the blade section at each spanwise position, consistent with Kelvin's theorem for the conservation of circulation, which provides with

2.1.3 Kinematic and dynamic conditions on the trailing vortex sheets of the blades

The velocity jump across each trailing vortex sheet S_w is tangential to these surfaces, and the pressure is continuous across this blade wake.

2.2 Numerical solution scheme

The blade and cavity surfaces and the trailing wakes of propeller blades are discretized by 4-

node hyperboloidal panels, where surface vorticity and sources of constant strength are distributed; see Fig.2. The problem, Eqs.(5) along with Kutta condition is solved at each time step, and the singularity distributions are calculated, from which velocity is computed from Eqs.(1) and (4). Once the velocities are found, the pressure distribution is obtained from Bernoulli's equation, as follows

$$\frac{p - p^{(I)}}{\rho} = -\frac{\partial \Phi}{\partial t} - \frac{1}{2} (|\mathbf{w}|^2 - |\mathbf{q} + \mathbf{A}|^2) = 0, \quad (6)$$

where $p^{(I)}$ denotes the incident field pressure in the moving coordinate system fixed to the propeller. For more details see Belibassakis & Politis (1998, 2002). Unsteady forces and moments, including thrust and torque, are subsequently calculated by pressure integration on propeller blades. The results concerning the thrust and torque coefficients are obtained as follows

$$K_T = T / (\rho n^2 D^4), \quad K_Q = Q / (\rho n^2 D^5), \quad (7)$$

where ρ is the density of the water, n the propeller revolutions per second, and D the propeller diameter.

3. Propeller blade cavitation

In the case of cavitating flow, the prescribed vapor pressure provides an additional criterion that controls the cavity formation and decay. Some important phenomena such as general cavity inception and surface tension are not considered. It is assumed that the cavity starts at the leading edge of the blade, and that only the suction side of the blade is cavitating (Lee, 1977, Kinnas et al 2003). The cavitating flow field is characterized by the following most important non-dimensional parameters, the cavitation number and the Froude number. The former is defined as follows

$$\sigma_n = (p - p_v) / (0.5 \rho n^2 D^2), \quad (8)$$

where p is the atmospheric and hydrostatic pressure at the propeller shaft center and p_v denotes the vapor pressure. The Froude number is also defined on the basis of the propeller rotational speed as follows

$$F_n = n^2 D / g, \quad (9)$$

where g is the gravitational acceleration.

3.1 Conditions on cavitating propeller

The problem concerning the unknown disturbance velocity and potential in the case of cavitating propeller is solved by imposing additional boundary conditions due to the presence of the cavity. Introducing a curvilinear coordinate system (u^1, u^2, u^3) as shown in Fig.3, and denoting by $h(u^1, u^2, t)$ the thickness of the cavity normal to the blade surface at the point (u^1, u^2) at time t , the Kinematic Boundary Condition (KBC) is used to determine the position of the cavity surface, given by the following equation,

$$\frac{D}{Dt} [u^3 - h(u^1, u^2, t)] = 0 , \quad (10)$$

where the material derivative appearing in the above equation is formulated in terms of the total flow velocity on the surface of the cavity.

Moreover, the Dynamic Boundary Condition (DBC) requires that the pressure, which is calculated using Bernoulli's equation (6), everywhere inside and on the cavity be constant and equal to the given cavity pressure

$$p = p_c . \quad (11)$$

3.2 Solution methodology

The cavity boundary is determined by an iterative process in which the dynamic boundary condition is satisfied on an approximate cavity surface and the kinematic boundary condition is used to update the surface. In the first iteration, the panels representing the cavity are placed on the foil surface. In subsequent iterations, the cavity surface is updated using the kinematic condition, and the boundary elements are moved to the updated surface.

The cavity extent on the blade (and wake) is found iteratively. After an initial guess based on the non-cavitating pressure distribution and cavitation number, the cavity thickness is computed. The local cavity length $\ell(u^2, t)$, defined as the arc length of the projection of the cavity (on the nose-tail axis along u^1) at each radial position $u^2 = \text{const}$ is determined from the following requirement (closure condition) at each spanwise strip

$$h(u^1 = \ell(u^1, t), u^2, t) = 0 . \quad (12)$$

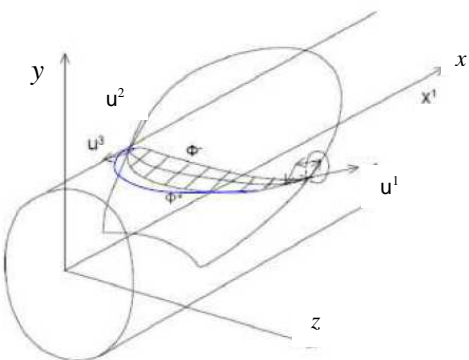


Fig. 3. Definition of the cavity surface on the suction side of the propeller blade

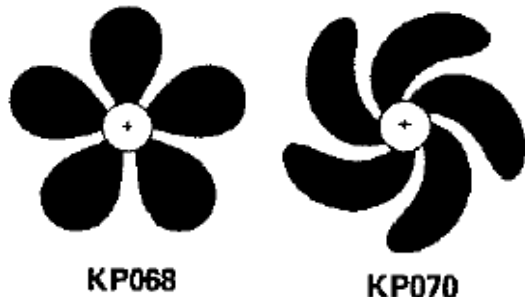


Fig.4 Unskewed and 70deg skewed propellers

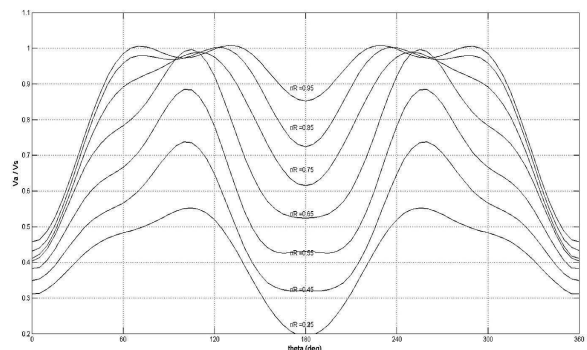


Fig.5 Distribution of axial wake at various radial positions from the hub to the tip of the propellers.

For a given cavitation number σ_n , the above requirement is used as the basis of an iterative solution scheme to calculate the cavity planform area and volume and its temporal variation.

As an example of application we consider two 5-bladed propellers, one without skew (KP068) and one with 70deg skew (KP070) for which detailed experimental data are available in Kim & Nguyen (1988); see Fig.4. The basic dimensions are: $D=0.25\text{m}$, $P/D=1.2$ (at 70% of tip radius), expanded area ratio 72.5%. The propellers operate in an axial wake. The angular distribution of the wake is shown in Fig.5 for various radial positions on the plane of the propellers.

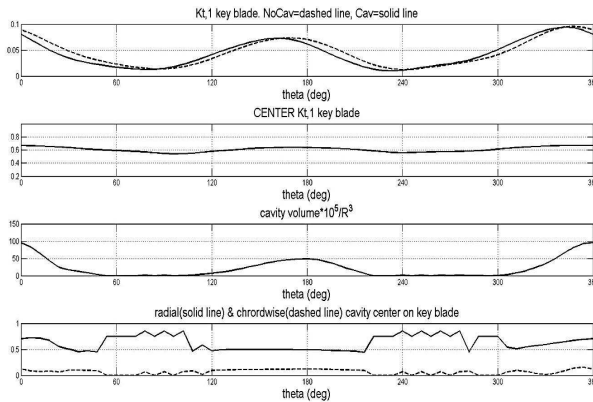


Fig. 6. Calculated results for the unskewed propeller (KP068) as obtained by the present method.

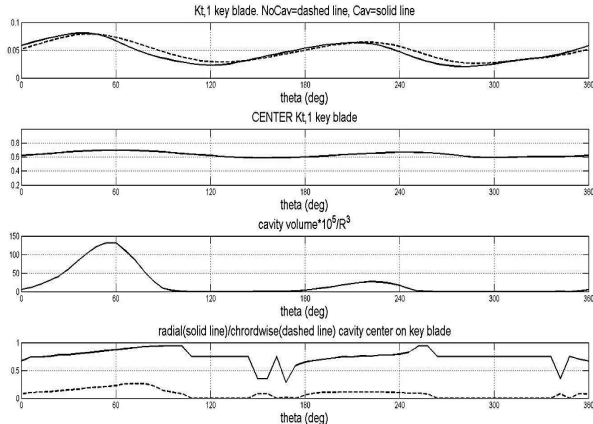


Fig. 7. Calculated results for the 70deg skewed propeller (KP070) as obtained by the present method.

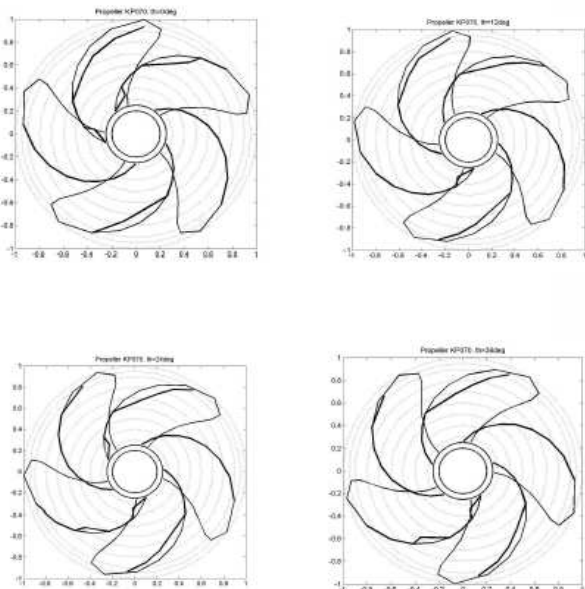


Fig. 8. Calculated cavitation extent on the blades of skewed propeller KP070 at various instances (angular positions).

The operating condition concerning the advance coefficient is $J=0.889$. Moreover, in the experiments the Froude number is $F_n = 12.34$ and the cavitation number is $\sigma_n = 3$. The calculated results for propeller KP068, as obtained by the present method, are presented in Fig.6 and for KP070 in Fig.7, respectively. More specifically, the first subplot in these figures shows the variation of the trust coefficient per blade in one revolution. Dashed lines indicate the result for non cavitating conditions and solid lines the modification due to blade sheet cavitation. In the second subplot the radial position of the center of thrust is plotted. In the third and fourth subplots the blade cavity volume and the coordinates of its center are shown, for the key blade at various angular positions. Moreover, in the case of the skewed propeller KP070, the calculated extent cavitation on blades is shown in Fig.8, at various instances (angular positions of the propeller). In general, present method predictions are found in good agreement with measured data (see Kim & Nguyen 1988).

5. Propeller noise prediction

As the propeller rotates, it is subjected to unsteady pressure loads, which lead to discrete tonal noise. Furthermore, blade cavitation significantly contributes to the generated acoustic spectrum. Thus, the underwater propeller noise is classified into cavitating and non-cavitating noise.

Low frequency noise is caused by the fluctuations of blade pressure and variation of unsteady sheet cavitation volume. The former has dipole characteristics and the latter is usually modelled by a bubble that acts as an acoustic monopole. High-frequency noise is caused by sheet cavity collapse and/or by shock wave generation.

The usual formulation for the acoustic pressure p' generated from rotating machinery is based on the Ffowcs Williams and Hawkings equation (FW-H) as follows

$$\frac{1}{c^2} \frac{\partial^2 p'}{\partial t^2} - \nabla^2 p' = m + d + q, \quad (13)$$

where c is the speed of sound in the medium ($c=1500-1550\text{m/s}$ for water) and the various terms in the right-hand side correspond to the

acoustic monopole, dipole and quadrupole source terms (Farassat & Myers 1988), defined as follows

$$m = \frac{\partial}{\partial t} [\rho u_n |\nabla f | \delta(f)] , \quad (14)$$

$$d = -\frac{\partial}{\partial x_i} [l_i |\nabla f | \delta(f)] , \quad (15)$$

$$q = -\frac{\partial^2}{\partial x_i \partial x_j} [T_{ij} H(f)] , \quad (16)$$

where $f=0$ indicates the moving surfaces u_n , the corresponding normal velocity, l_i the loads and T_{ij} the stresses. The quadrupole term becomes important for strongly transonic flow phenomena at higher frequencies. Taking into account that the speed of sound in water is much greater than the flow velocities, and focusing on the low-frequency part of the generated noise spectrum the contributions by the latter term are neglected in the present work. In the sequel Farassat formulation 1A (Farassat 2001, Seol et al 2005) is employed offering an integral representation of the solution of Eq.(13) forced by the monopole and dipole terms. The acoustic pressure field is accordingly given by thickness and loading components, as follows

$$p'(\mathbf{x}_0, t) = p'_T(\mathbf{x}_0, t) + p'_L(\mathbf{x}_0, t) . \quad (17)$$

The loading term is given by

$$4\pi p'_L(\mathbf{x}_0, t) = -\frac{1}{c} \frac{d}{dt} \int_{f=0} \left[\frac{dp \hat{\mathbf{n}} r}{r(1-M_r)} \right]_{ret} dS + \int_{f=0} \left[\frac{dp \hat{\mathbf{n}} r}{r^2(1-M_r)} \right]_{ret} dS , \quad (18)$$

where dp denotes the pressure jump on the blade surface, M_r denotes Mach number in the r -direction (see Fig.1) and the integrand is calculated at retarded time. For relatively large distances (of the order of several propeller diameters) of the observation point from the propeller, we use the approximation

$$r = |\mathbf{x}_0 - \mathbf{x}| \approx |\mathbf{x}_0 - \mathbf{x}_{T,k}(t)|, \quad \hat{r} \approx (\mathbf{x}_0 - \mathbf{x}_{T,k}(t))/r$$

where $\mathbf{x}_{T,k}(t)$ denote the center of thrust on the k -blade, which is the most important load of the lifting surface. Using the fact that the Mach number is very small, Eq.(18) leads to the following simplification

$$p'_L(\mathbf{x}_0, t) = -\frac{1}{4\pi c} \sum_{k=1}^Z \frac{d\tilde{T}_k(t_r)}{dt} \frac{x_p - x_{T,k}(t_r)}{r^2} + \frac{1}{4\pi} \sum_{k=1}^Z \tilde{T}_k(t_r) \frac{x_p - x_{T,k}(t_r)}{r^3}, \quad (19)$$

where $\tilde{T}_k(t_r)$ denotes the fluctuating unsteady part of the k -blade thrust, as e.g. shown in the first subplots of Figs.6 and 7 for propellers KP069 and KP00, and $t_r = r/c$ denotes the retarded time between the observation point \mathbf{x}_0 and the disturbance generating point $\mathbf{x}_{T,k}$.

Similarly, for the thickness effect we have

$$4\pi p'_T(\mathbf{x}_0, t) = \rho \frac{\partial}{\partial t} \int_{f=0} \left[\frac{u_n}{r(1-M_r)} \right]_{ret} dS. \quad (20)$$

Considering the same as before approximations, Eq.(20) is simplified in the following form

$$4\pi p'_T(\mathbf{x}_0, t) \approx \frac{\rho}{r} \frac{\partial}{\partial t} \int_{f=0} [u_n]_{ret} dS. \quad (21)$$

Moreover, we consider that the blades are very thin in comparison to the cavity, and using

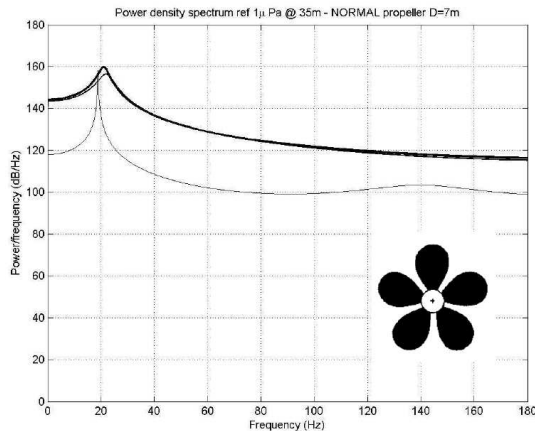
$$\int_{f=0} u_n dS \approx \frac{dQ_c(t)}{dt}, \quad (22)$$

where $Q_c(t)$ denotes the cavity volume, as e.g. shown in the third subplots of Figs.6 and 7, we finally obtain

$$p'_T(\mathbf{x}_0, t) \approx \frac{\rho}{4\pi} \sum_{k=1}^Z \frac{d^2 Q_{c,k}(t_r)}{dt^2} \frac{1}{|\mathbf{x}_0 - \mathbf{x}_{Q,k}(t_r)|} , \quad (23)$$

where $\mathbf{x}_{Q,k}(t)$ denotes the center of cavity volume of the k -blade.

Calculations based on the above approximate formulas, Eqs. (19) and (23), significantly reduce the computation cost of the surface integrals (18) and (21), respectively. Numerical results are presented in Figs.9 and 10 for the KP060 and KP070 propellers, respectively, rescaled from model to full dimension with diameter $D=7$ m. More specifically, the top subplot of Fig.9 shows the frequency spectrum with reference to $1\mu\text{Pa}/\text{Hz}^2$ for the KP068 unskewed propeller. Thin solid line



load and cavity non cavitating

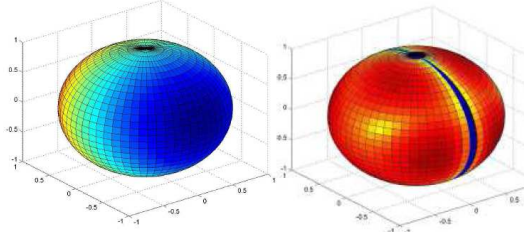
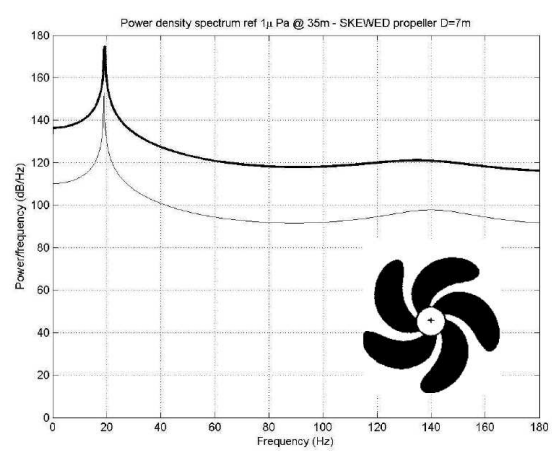


Fig.9 Frequency spectrum of propeller KP068 rescaled to $D=7\text{m}$ (top) and directional pattern (bottom).

indicates the contribution of the propeller loading term, which essentially corresponds to the non-cavitating condition. Thick line indicates the total noise spectrum of the unskewed propeller (rescales to $D=7\text{m}$) operating in cavitating conditions. In the same figure the colorplots indicate the directivity characteristics of the propeller noise for the above considered conditions, estimated by the total energy of the frequency spectrum at points on the surface of a sphere at a distance of 10 propeller diameters. Corresponding results concerning the skewed propeller are shown in Fig.10. We clearly observe in these figures the appearance of the peak of the noise spectrum at the blade frequency, which is more sharp in the case of the skewed propeller. Also, it is evident that cavitation significantly modifies (about 20dB/Hz in this example) the levels of the acoustic spectral density.

The directivity pattern is further modified by the presence of additional boundaries. In particular, the effect of the free surface, as a pressure release boundary, modifies significantly the noise pattern at



load and cavity non cavitating

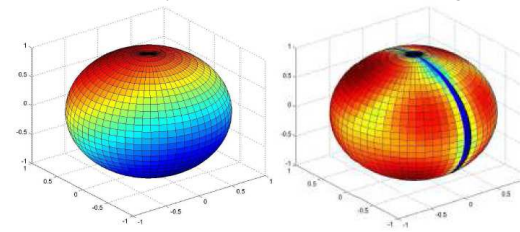


Fig.10 Frequency spectrum of propeller KP070 rescaled to $D=7\text{m}$ (top) and directional pattern (bottom).

further distances due to Lloyd mirror effect, as e.g. illustrated in AQUO (2015, Annex 2), and should be take into account.

Moreover, the hull boundary has also a significant effect in the modification of the directivity characteristics of the noise generated by the propeller. In order to demonstrate this effect, we consider a simple (monopole) harmonic source at frequency 65Hz (center of the first octave band), and the acoustic field generated taking into account the reflective characteristics of the hull. As an example, we consider an elongated body in the form of a prolate spheroid with length 100m and breadth 15m, with the propeller acting as a monopole source at a small distance from the stern. Numerical results are presented in Figs.11 and 12, modeling the hull surface as a hard surface (Neumann boundary conditions) and as a soft surface (Dirichlet boundary condition), respectively. It is clearly observed in these plots that the directivity characteristics of acoustic field are strongly modified, especially in the case of the soft hull boundary by the effect of the hull. In particular, the acoustic energy propagating in the forward direction (at the depth level of the source) is smaller than the corresponding one propagating in the backward direction of the travelling vessel.

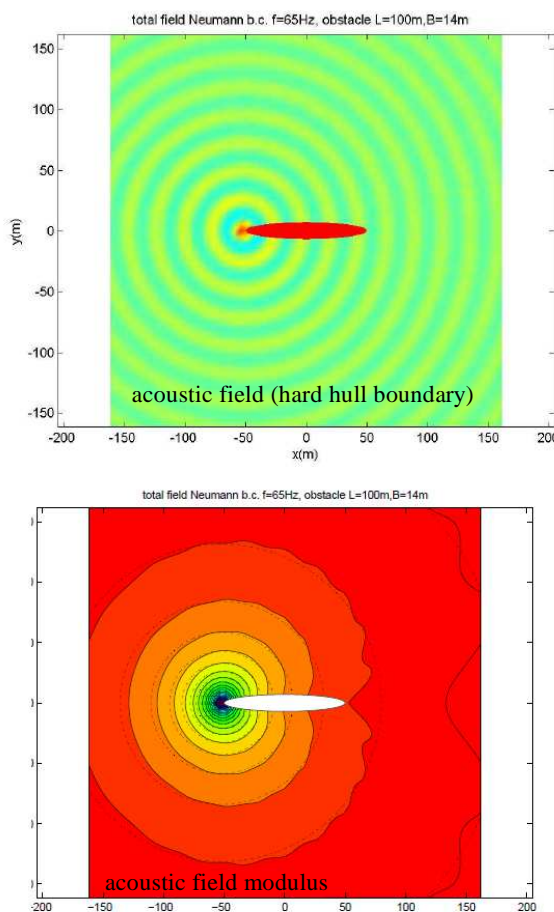


Fig.11. Modification of the directivity characteristics of the acoustic field by a point harmonic source from the presence of a hard boundary (hull).

5. Conclusions

A numerical model is developed for the prediction of non-cavitating and blade sheet cavitation noise generated from marine propellers, operating in unsteady inflow conditions at the stern of the ship. The hydrodynamic part is analyzed by a velocity-based panel method, providing the unsteady pressure on the blades and cavitation data. The latter are subsequently used, in conjunction with Farassat formulation, to calculate acoustic radiation from moving surfaces and predict the acoustic spectrum at a distance of several diameters from the propeller, representing the source of marine propeller noise. At a first level of approximation, a reduced-order model is derived, exploiting information and integrated data concerning the time history of blade sheet cavity volume and the unsteady blade thrust.

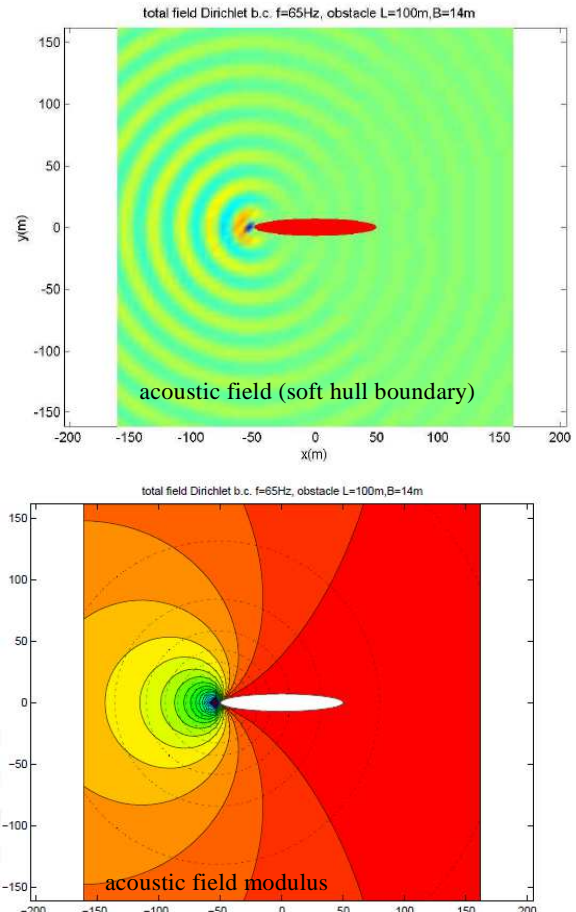


Fig.12. Modification of the directivity characteristics of the acoustic field by a point harmonic source from the presence of a soft boundary (hull).

Results concerning cavity volume and blade thrust variations are used to calculate the monopole and dipole components of the propeller acoustic spectrum in the low and moderate frequency band. Also, the directivity characteristics of the ship propeller are calculated, and the effect on underwater noise propagation is presented comparatively to the omnidirectional source assumption. Future work will be directed to the validation of the proposed simplified method by comparison to full calculations as well as experimental measured data.

Acknowledgement

This study was undertaken in the frame of the project MEDCIS: Support Mediterranean Member States towards Coherent and Coordinated Implementation of the second phase of the MSFD, funded by the European Commission, DG Environment, Grant agreement 11.0661/2016/748067/SUB/ENV.C2, Coordinator Dr. K. Pagou.

References

- [1] J.A.Hildebrand. Anthropogenic and natural sources of ambient noise in the ocean, Mar Ecol Prog Ser, 395 (2009) 5–20.
- [2] M.F. McKenna, D. Ross, S.M. Wiggins, J.A. Hildebrand. Underwater radiated noise from modern commercial ships, J Acoust Soc Am. 131 (2012) 92-103.
- [3] AQUO 2015. Ship Underwater Radiated Noise Patterns, (2015). Report R2.9 Achieve Quieter Oceans by shipping noise footprint reduction (FP7 Collaborative Project No314227).
- [4] IMO 2014. Guidelines for the Reduction of Underwater Noise from Commercial Shipping to Address Adverse Impacts on Marine Life – non mandatory technical advices, International Maritime Organization (2014) MEPC.1/Circ.833.
- [5] G. Frisk. Noiseconomics: The relationship between ambient noise levels in the sea and global economic trends, Scient. Reports (2012) 2, Art.: 437, (<https://www.nature.com/articles/srep00437>).
- [6] D.Wittekind, M. Schuster. Propeller Cavitation Noise and Background Noise in the Sea, proceedings 1st Inter. Meeting - Propeller Noise & Vibration 6-7 November 2014, Istanbul, Turkey.
- [7] IMO 2009. Noise from commercial ships and its adverse impact on marine life Rep. Marine Environment Protection Committee MEPC 59/19.
- [8] S. Kinnas, Y.L.Young. Modeling of Unsteady Sheet Cavitation on Marine Propeller Blades, Intern.Journal of Rotating Machinery Taylor & Francis Inc, 9 (2003) 263–277.
- [9] H.Seol, J.C. Suh, S.Lee. Development of hybrid method for the prediction of underwater propeller noise. Journal of Sound and Vibration 288 (2005) 345–360.
- [10] K.A.Belibassis, G.K.Politis. A non-linear velocity based Boundary Element Method for the analysis of marine propellers in unsteady flow, International Shipbuilding Progress 45 (1998) 93-133.
- [11] K.A. Belibassakis, G.K. Politis. Unsteady performance of propellers with non-conventional blade geometry by a vorticity based panel method, Proc.10th Congress of Intern. Maritime Association of the Mediterranean, IMAM 2002, Rethymnon-Crete.
- [12] F. Farassat, M.K., Myers. Extensions of Kirchhoff's formula to radiation from moving surfaces, Journal of Sound and Vibration 123 (1988) 451–460.
- [13] F. Farassat. Acoustic radiation from rotating blades – the Kirchhoff method in aeroacoustics, Journ. of Sound and Vibration 239(2001) 785-800.
- [14] G.K. Politis. Simulation of unsteady motion of a propeller in a fluid including free wake modeling. Engineering Analysis with Boundary Elements 28 (2004),633–53.
- [15] J. Kerwin, C.S Lee. Prediction of steady and unsteady performance of marine propellers by numerical lifting surface theory, SNAME Transactions 86 (1978).
- [16] C.S. Lee. Prediction of Steady Unsteady Performance of Marine Propellers With or Without Cavitation by Numerical Lifting Surface Theory, PhD Thesis, MIT, Department of Ocean Engineering, 1979.
- [17] T. Hoshino. Numerical and experimental analysis of the propeller wake using a surface panel method and a 3-component L.D.V., Proc. 18th Symp. on Naval Hydrodynamics 1990.
- [18] K.H. Kim, P.H. Nguyen. Propeller cavitation and cavitation induced pressure fluctuation: Comparison between theory and experiments. Proc. SNAME Propellers'88 Symposium (1988) Virginia Beach.